PETROPHYSICS, VOL. 59, NO. 2 (APRIL 2018); PAGES 136–152; 9 FIGURES; 1 TABLE. DOI: 10.30632/PJV59N2-2018a2

Nuclear Magnetic Resonance and Pore Coupling in Clay-Coated Sandstones With Anomalous Porosity Preservation, Água Grande Formation, Recôncavo Basin, Brazil

Marta H. Jácomo[1], Ricardo I.F. Trindade[1], Everton L. de Oliveira[2], Carlson de M. M. Leite[3], Elton Tadeu Montrazi[2], Mariane Andreeta[2], Tito J. Bonagamba[2]

ABSTRACT

Continuous chlorite coats are known to preserve the porosity in deeply buried sandstones by forming physical barriers to quartz early overgrowth. Sandstones from Água Grande Formation, Recôncavo Basin, Brazil, present anomalous porosity due to development of chlorite coating and is therefore suited for studying the nuclear magnetic response to this effect. Samples from this unit were classified into three groups according to their texture, composition and abundance of chlorite coatings: Group 1 with low amounts of coating, Group 2 with high amounts of coating and a nonreservoir sample (Group 3). Group 1 samples show wide NMR T_2 distribution, while Group 2 samples present a bimodal T_2 distribution. Nonreservoir Group 3 samples showed only a T_2 peak in much shorter T_2 times. To interpret the NMR results, transmitted-light optics, scanning electron microscopy, porosity (ϕ) and permeability (k) measurements, micro-CT, X-ray diffraction, magnetic susceptibility and hysteresis were used. We conclude that the longest T_2 (> 0.1 s) peak of reservoir samples (Groups 1 and 2) is due to intergranular macropores, the intermediate peak is due to feldspar or clay intraclasts dissolution and the shortest peak (~0.01 s) is due to the chlorite coating itself, with minor contribution from secondary microporosity. The microporosity is predominant in the nonreservoir sample and relates to the clay-bound water. The shift to shorter times of longer T_2 peaks in samples with higher contents of chlorite-bearing sandstones is likely related to diffusive coupling.

INTRODUCTION

Good porosity preservation is a key parameter in hydrocarbon reservoir exploration, particularly in deep reservoirs (> 4 km). The loss of porosity with increasing depth is due to mechanical and chemical compaction, in addition to secondary cementation. However, clay coatings on detrital host grains, when present as infiltrated clays in sandstones, even in small volumes, can inhibit quartz overgrowth, thus preserving the porosity at depth (Moraes and De Ros, 1990; Anjos et al., 2003). Bloch et al. (2002) have defined porosity preservation after burial as an "anomalous porosity" condition.

Several studies have shown that early chlorite coatings on detrital grains are correlated with porosity preservation in deep reservoirs. However, there is no consensus on the way in which it contributes to preservation. While some authors affirm that chlorite grains inhibit the growth of quartz by separating the detrital-grain surface to pore water, preventing the dissolution of the grains and avoiding nucleation (Ehrenberg, 1993), others suggest that inhibition of quartz overgrowth occurs due to limited epitaxial growth of interparticle space by clay (Billault et al., 2003; Ajdukiewicz and Larese, 2012).

Anomalous porosities are observed only in sandstones containing eodiagenetic precompaction clays, which can be chloritized during mesodiagenetic processes. Late and neoformed mesogenetic clay coatings do not preserve the porosity, since sediments would have been submitted to the conditions necessary for cementation. An exception to this rule would be the formation of chlorite by the direct precipitation of interstitial fluids (Morad et al., 2000; Berger et al., 2009).

Chlorite is the most effective coating to produce anomalous porosity, but some studies have reported porosity preservation in fluvial reservoir rocks with chlorite, which is a precursor of smectite (e.g., McKinley et al., 2003; Worden and Morad, 2003; Luo et al., 2009). Early diagenetic chlorite grains form on the interface between the detrital grains and the intergranular porous space, while other clays, such as smectite, grow perpendicular to the grain, forming a pore-bridging texture (Pitmann et al., 1992). Chlorite particles

Manuscript received by the Editor September 27, 2017; revised manuscript received January 8, 2018; manuscript accepted January 10, 2018.
[1]Universidade de São Paulo, Instituto de Astronomia, Geofísica e Ciências Atmosféricas, Departamento de Geofísica, Rua do Matão, 1226, São Paulo, Brazil; marta.jacomo@gmail.com; rtrindad@iag.usp.br
[2]Instituto de Física de São Carlos, Universidade de São Paulo, Av. Trabalhador são-carlense, 400 - Pq. Arnold Schimidt, São Carlos, Brasil; everton.lucas.oliveira@usp.br; elton.montrazi@usp.br; mariane.ceres@gmail.com; tito@ifsc.usp.b
[3]PETROBRAS, Unidade de Operação-BA, Exploração. Avenida Antonio Carlos Magalhães, 1113, Edifício Torre Pituba, 20º Andar Salvador, Bahia, Brasil; cmml@petrobras.com.br

that are parallel or slightly oblique to the detrital surface tend to orient themselves progressively perpendicularly with increasing distance from the grain boundary due to geometric selection. During particle growth, the particles compete for available space such that some oriented crystals gain favorably more growth space than others. In this process, only high-tilting or perpendicular crystals continue to grow, as nothing can inhibit the growth of these crystals, since there is no competition among them (Ajdukiewicz and Larese, 2012).

Despite numerous works on the clay-coating structure, mineral texture and the mechanisms leading to porosity preservation, a detailed study of the porosity distribution and macropore to micropore connection in these rocks is still lacking. Here, we apply nuclear magnetic resonance (NMR) techniques that allow us to investigate the pore-size distribution and the possible connection between pore families, together with other techniques for the pore-space investigation, such as transmitted-light optics, scanning electron microscopy and microcomputed tomography. We analyzed fluvial and eolian sandstones from the Água Grande Formation in the Recôncavo Basin, comprising samples with anomalous porosity due to the presence of clay coats and microquartz (Leite et al., 2014), and a nonreservoir sample. These eolian and fluvio-eolian sandstones are excellent oil-producing reservoirs in the Recôncavo Basin, even under deep burial conditions.

METHODS

The pore space and the fluid, which fills the pores, control the NMR transverse (T_2) and longitudinal (T_1) relaxation processes by three mechanisms:

1. T_1 and T_2 intrinsic relaxations, which are mostly controlled by viscosity, fluid composition, temperature and pressure;
2. T_1 and T_2 surface relaxations, which are controlled by grain mineralogy and S/V ratio (size/ volume of pores); and
3. T_2 relaxation is affected by molecular diffusion, which is controlled by the behavior of the fluids when subjected to a magnetic field gradient; in this case, molecules diffuse into areas with distinct magnetic fields, making the precession rates different.

The relation that governs surface mechanisms in the fast-diffusion regime (Brownstein and Tarr, 1979; Kenyon, 1997) is:

$$1/T_1 = \rho_1(S/V) \text{ and } 1/T_2 = \rho_2 (S/V), \quad (1)$$

where ρ_1 and ρ_2 are the pore surface relaxivities for T_1 and T_2, respectively; S/V is the surface/volume ratio. Surface relaxivity can be interpreted as a measurement of how much the proton magnetization can relax when it encounters a pore surface and depends on the concentration of paramagnetic impurities and magnetic particles on it. At first approximation, the larger the pore size the smaller the S/V ratio, and the longer the relaxation time T_2.

The total magnetization is the sum of decay signals of each pore size:

$$M_z(t) = \sum_{i=1}^{n} M_i \exp(-t/T_{2i}) \ , \quad (2)$$

where M_i is the equilibrium magnetization, T_{2i} is a constant decay time for the *ith* pore and $M_z(t)$ is the total magnetization at time t.

The relaxation-time rate due to molecular diffusion in a gradient magnetic field is given by:

$$\frac{1}{T_{2diffusion}} = \frac{D(\gamma GTE)^2}{12} \ , \quad (3)$$

where $1/T_{2diffusion}$ is the relaxation rate due the molecular diffusion, D (cm^2/s) is the molecular diffusion coefficient, γ is the gyromagnetic ratio, G is the magnetic field gradient (G/cm) and TE is the interecho time used in the Carr-Purcell-Meiboom-Gill (CPMG) sequence measurements.

T_1, T_2 and D-T_2 measurements were done on samples saturated with fresh water. Inversion-recovery, CPMG and PFG-STE + CPMG sequences were used for for T_1, T_2 and D-T_2 analysis, respectively (Song et al., 2002; Mitchell et al., 2013).

The CPMG measurements were performed with echo times of 200 μs with 32 averages for each experiment. The 2D D-T_2 experiment was performed on the 2-MHz equipment, with time to the fixed stimulated echo of 6 ms, diffusion time of 40 ms, and time to the Hahn echo of 200 μs.

To convert the decay functions into a T_2 distribution we used the inverse Laplace transform (ILT) implemented in an in-house program developed in the NMR Group. Two-dimensional maps were constructed with a patented MATLAB routine developed by Schlumberger Ltd.

^{1}H NMR measurements were performed using two Redstone Tecmag spectrometers, one operating at 2 MHz and another at 85 MHz, using a permanent magnetic (0.047 T) and an Oxford Instruments superconductor magnet (2 T), respectively, both from Instituto de Física de São Carlos, Universidade de São Paulo.

Complementary to the NMR study, we used transmitted-light optical and electron microscopy (SEM), gas porosimetry and permeametry, micro-CT (μCT), X-ray diffraction (XRD) and hysteresis measurements in order to identify and characterize the texture and reservoir properties of the samples. A detailed description of the experimental conditions and equipment used in these measurements is provided in Appendix 1.

THE ÁGUA GRANDE FORMATION, RECÔNCAVO BASIN

Recôncavo Basin is an aborted rift half-graben rift situated in Northeastern Brazil, related to the South Atlantic Ocean opening during the Early Cretaceous (Milani and Davison, 1988). It is one of the most productive onshore areas in the country, with 72 mature fields presently in operation (ANP, 2016). Recôncavo basin reservoirs can be categorized into three main groups: (1) prerift eolian fluvial sandstones of the Sergi and Água Grande formations; (2) synrift deltaic sandstones of the Ilhas Group; and (3) synrift turbidite sandstones of the Candeias and Maracangalha formations. The prerift system comprises the main reservoirs. The Candeias Formation is the hydrocarbon source for the petroleum system. It consists of organic-rich grayish lacustrine shales (average 4% TOC and Type I kerogen) intercalated with mudstones, siltstones, limestones and dolomites (Magnavita et al., 2012).

Reservoir rocks of the Água Grande Formation are eolian-fluvial sequences. The fluvial unit is composed of fining upward cycles with conglomeratic sandstones at the base, grading from coarse to fine sandstone and capped by silty shales. The eolian unit is composed of well-sorted medium grained planar-bedded sandstones with depositional structures, which are typical laminations of depositional processes. (Cortez, 1996). This progradational context has been interpreted as a drying upward cycle by Wiederkehr (2010).

RESULTS

Petrography, Electronic Microscopy and X-Ray Diffraction

We analyzed eight core plugs from Água Grande Formation sandstones, comprising seven plugs from the stratigraphic interval characterized by anomalous porosity by Leite et al. (2014) and one nonreservoir sample. We divided the studied samples into three groups according to their sedimentary texture and composition (Table 1).

Group 1 comprises samples 7560, 7564 and 7570. They consist of moderately- to well-sorted subarkose or quartz sandstones, which are composed of quartz and feldspar as primary minerals. The diagenetic minerals are kaolinite and quartz overgrowth cements, which fill the pores. Dissolution of feldspar and clay intraclasts contributes a significant portion of the porosity, varying from 1.3 to 5.0% (see Appendix 2).

Table 1—Petrophysical Parameters for Água Grande Formation Samples

Sample No. Depth (m)	Texture Original (Folk, 1968)	Depositional Environment (Geological Description)	Group	Porosity (Petrography) (%)	Porosity (Density) (%)	Porosity (Helium) (%)	Permeability (Helium) (mD)	Magnetic Susceptibility (10^{-6} SI)	Petrofacies
7560 1,705.75	Quartz sandstone	Fluvial – deep burial diagenesis	1	15.00	10.08	10.40	9.87	19.27	Low-permeability fluvial
7564 1,706.70	Subarkose	Fluvial – shallow to deep mesodiagenesis	1	9.66	9.17	10.20	7.52	24.26	Low-permeability fluvial
7570 1,707.85	Subarkose	Fluvial	1	9.00	8.44	10.80	44.70	8.05	High-permeability fluvial
7536 1,699.65	Subarkose	Eolian – sand sheet with fluvial incursions or fluvial bars with eolian reworking	2	20.67	19.96	20.80	34.30	31.10	High-pemeability Eolian
7545 1,701.95	Subarkose	Fluvial-eolian – shallow to deep mesodiagenesis	2	19.67	15.27	17.30	4.14	29.88	Low-permeability Fluvio-eolian
7549 1702.80	Quartz sandstone	Fluvial – deep burial diagenesis	2	23.33	16.75	18.00	8.40	45.92	Low-permeability fluvial
7552 1703.50	Subarkose	Fluvial– deep burial diagenesis	2	18.00	17.00	17.70	4.69	31.07	Low-permeability fluvial
7562 1,706.10	Mud sandstone (textural)	Fluvial – deep burial diagenesis (deep mesodiagenesis)	3	0.00	2.77	1.40	0.00	116.67	Nonreservoir

Group 2 comprises samples 7536, 7545, 7549, and 7552, which are characterized by moderately- to well-sorted subarkoses or quartz sandstones with parallel laminations. While quartz and feldspar are primary minerals, the diagenetic minerals are dickite, anatase, quartz overgrowth, dolomite, chalcedony and albite (see Appendix 2). Pore-filling minerals, such as dickite and anatase, are the main cause of porosity loss in these petrofacies. Similar to Group 1 samples, feldspar and the clay intraclasts were partially dissolved and developed secondary macroporosity, corresponding to 2.0 to 4.7% of porosity volume. Intragranular diameter pores vary from 10 to 30 µm.

All reservoir samples have some content of clay coating on the host grains (Fig. 1). X-ray diffraction (XRD) was used to identify the clay types. As the amount of clay coats from Group 1 is below the detection limit, Fig. 2 shows the XRD results only from Group 2. Chlorite coating is evident by the ~14 Å peak in natural conditions (Line 1) and the 15 Å peak in ethylene glycol (Line 2). It does not show the expansion from 16.65 to 17.15 Å under ethylene glycol solution, which is typical of smectite (Srodon, 1980; Beaufort et al., 1997). Kaolinite is present in all samples (Groups 1 and 2).

Authigenic chlorite occurs as pore-lining crystals, whose flakes are 5 to10 µm across with a thickness of ~0.1 µm and sometimes behave like pore-bridging clay, reducing the throats of pores and consequently the permeability (Figs. 1e to 1h). The eolian Sample 7536 of Group 2 presents much less developed perpendicular flakes than the other samples (Figs. 1e and 1h). Group 1 presents less coating than Group 2 samples. When chlorite coatings are poor, discontinuous or absent, overgrowth of quartz cement occurs and part of the porosity is lost (Figs. 1b and 1i). Figure 1h shows that when the quartz overgrowth is perpendicular to the host grain (outgrowth), chlorite does not prevent quartz overgrowth as proposed by Ajdukiewicz and Larese (2012).

To estimate the chlorite amounts, the SEM composition maps were combined into a color image (Fig. 3). Typically, Group 1 samples show less chlorite content in comparison to Group 2 samples (Fig. 3), with the percent of iron on grain surfaces between 5 and 31% in the former, and between 39 and 60% in the latter. The only exception is Sample 7560, which is part of Group 1 but presents 50% iron covering the host grains.

Group 3 is the nonreservoir sample. It consists of fine and moderately sorted mud sandstone (25% mud) with long or concave-convex contacts, attesting to significant pressure dissolution and the porosity loss (Table 1). This facies is composed of primary quartz and feldspar. Diagenetic minerals include dickite, illite/smectite, chlorite, anatase and pyrite (see Appendix 2). SEM images (Fig. 1j) and thin sections do not show any chlorite or chalcedony/

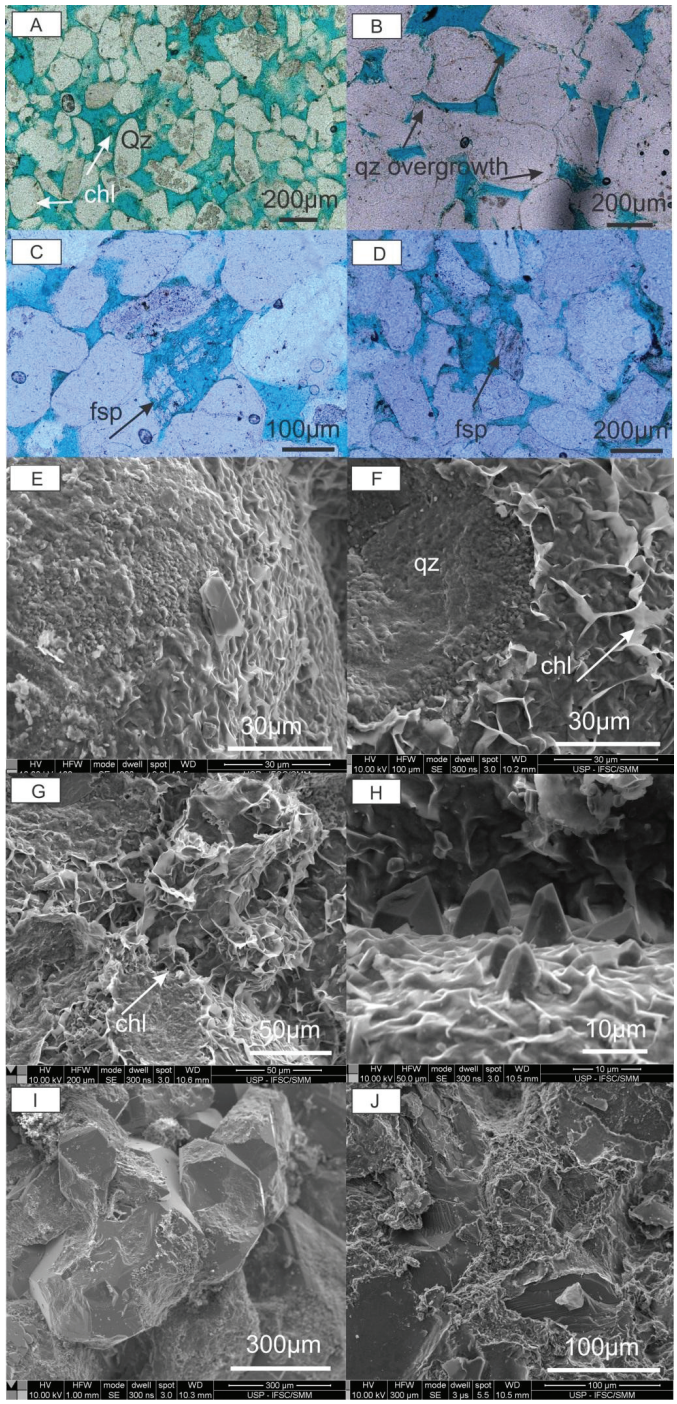

Fig. 1—Optical and SEM images showing chlorite (chl) coating over quartz (qz) grains. Optical microscope images show the higher amount of coating in Group 2 samples (a) than in Group 1 samples (b). Group 1 samples develop quartz overgrowth (b). (c and d) show some examples of feldspar (fsp) dissolution generating secondary porosity in samples from both Groups. SEM images of chlorite coats with honeycomb morphology forming pore lining clays (e, f, h), sometimes with morphology similar to corrensite (chlorite-smectite) developing pore bridging (g). Sample 7570 in (i) shows almost no chlorite coating (i). Nonreservoir Sample 7562 (j) is very cemented and presents very low porosity and almost no permeability.

microcrystalline coatings.

Porosity (ϕ), Permeability (k) and Pore-Size Distribution

Porosity estimations with helium porosimetry for Group 1 samples vary from 10.2 to 10.8%. These results agree with those obtained by other methods, including thin-section point counting and density measurements (Table 1). Permeability for the same samples is within 7.52 and 9.87 mD for low-permeability samples (7560 and 7564) and 44.7 mD for the high-permeability sample (7570) (Table 1). Group 2 contains chlorite and preserves a good porosity, varying from 17.7 to 20.8% (helium porosimetry). The permeability in this group of samples varies from 4.13 to 8.40 mD for fluvial samples, and is 34 mD for the eolian sample. The nonreservoir Group 3 sample is strongly cemented and presents very low porosity (1.4%) and no permeability.

Pore-size distribution was estimated through μCT. Pore sizes vary from 32.67 to 36.35 μm in Group 1, and from 24.68 to 33.98 μm in Group 2, but both groups have similar modes (volume versus pore size) of ~20 μm regardless of grain size (Fig. 4a). Pore-size distributions were modeled using a digital rock reconstruction of μCT images and a pore-throat network technique developed by Andreeta (2017) (Fig. 4b). According to the model, Group 2 pore sizes present unimodal size distributions (Fig. 4c) even when grains have a bimodal texture, confirming the μCT data.

Magnetic Susceptibility and Hysteresis

Group 1 samples show lower magnetic susceptibility than Group 2 samples. Susceptibility values vary from 8.05×10^{-6} to 24.26×10^{-6} SI in Group 1, and from 29.88×10^{-6} to 45.92×10^{-6} SI in Group 2. For most samples from both groups, hysteresis data show that the paramagnetic signal of clays is dominant (Figs. 5a to 5e).

A very small amount of low-coercivity magnetic minerals can be detected in the hysteresis cycle, probably due to trace amounts of magnetite (Figs. 5a to 5e). For Sample 7570, which shows the smallest content of clay coating, the magnetic susceptibility at higher field is negative, and directly related to the quartz matrix (Fig. 5f). Since the magnetic susceptibility, particularly at fields above 0.1 T, is almost completely controlled by the paramagnetic clays, it

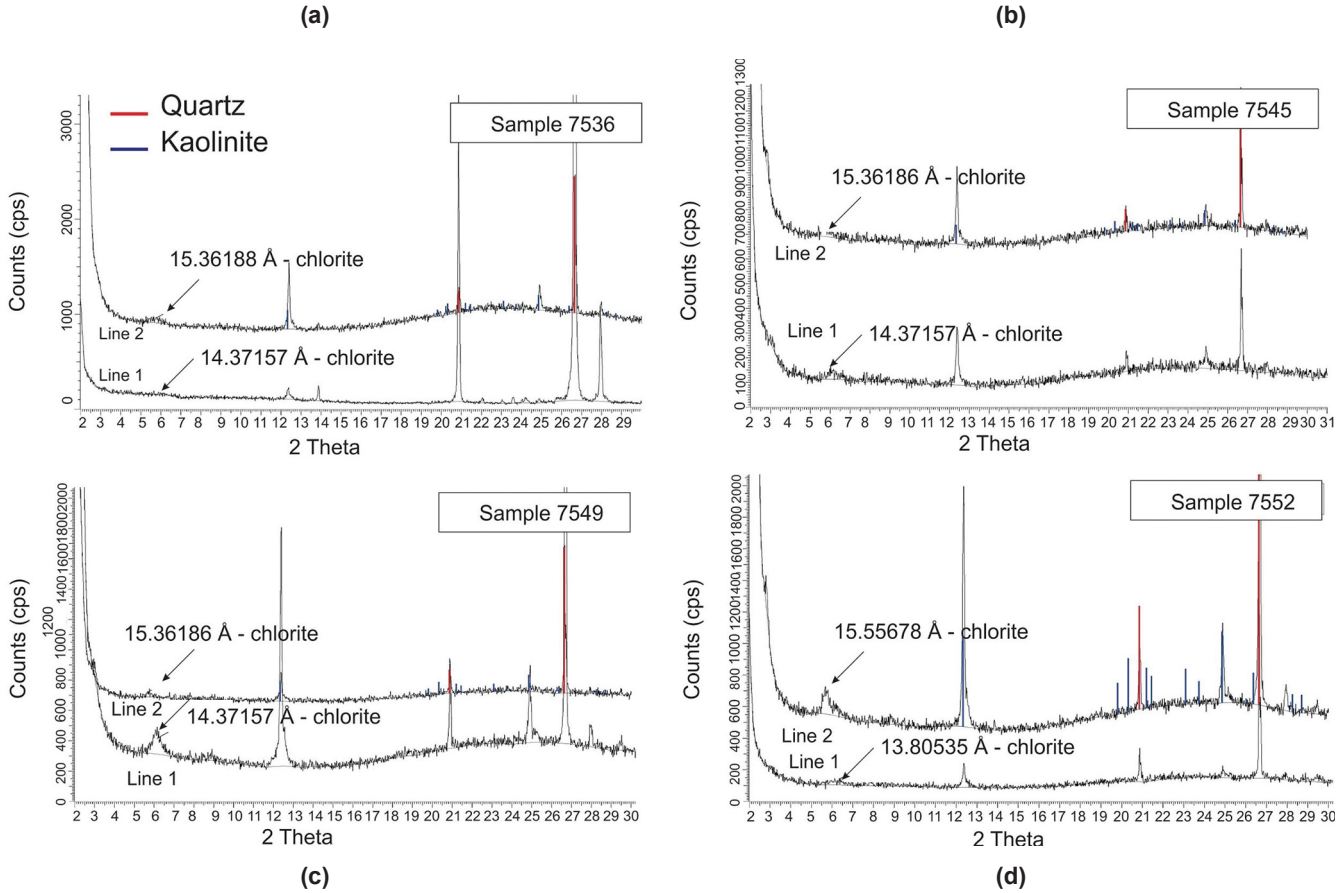

Fig. 2—XRD spectrum of Group 2 reservoir samples showing chlorite, kaolinite and quartz peaks. (a) Sample 7538, (b) Sample 7545, (c) Sample 7549, and (d) Sample7552.

can also be used as an indicator of the amount of chlorite coating in these samples. The Group 3 sample shows the highest magnetic susceptibility of 116.67x10^{-6} SI.

Nuclear Magnetic Resonance

Figure 6 shows T_2 relaxation time distributions for all studied samples. Group 1 samples show a wide distribution of T_2 values. The best log-gaussian fittings to the T_2 distribution shows three defined sites: the shortest varies from 0.025 to 0.01 s; the intermediate from 0.02 to 0.1 s; and the longest from 0.1 to 0.44 s. In contrast, Group 2 samples present two well-defined modes in the T_2 time distribution whose peaks vary from 0.016 to 0.018 s for the shortest times, and from 0.19 to 0.209 s for the longest times. In the nonreservoir sample (Group 3), the micropores with T_2 time mode at 0.001 s predominates. Very low intensity peaks also occur at 0.02 s and 0.576 s.

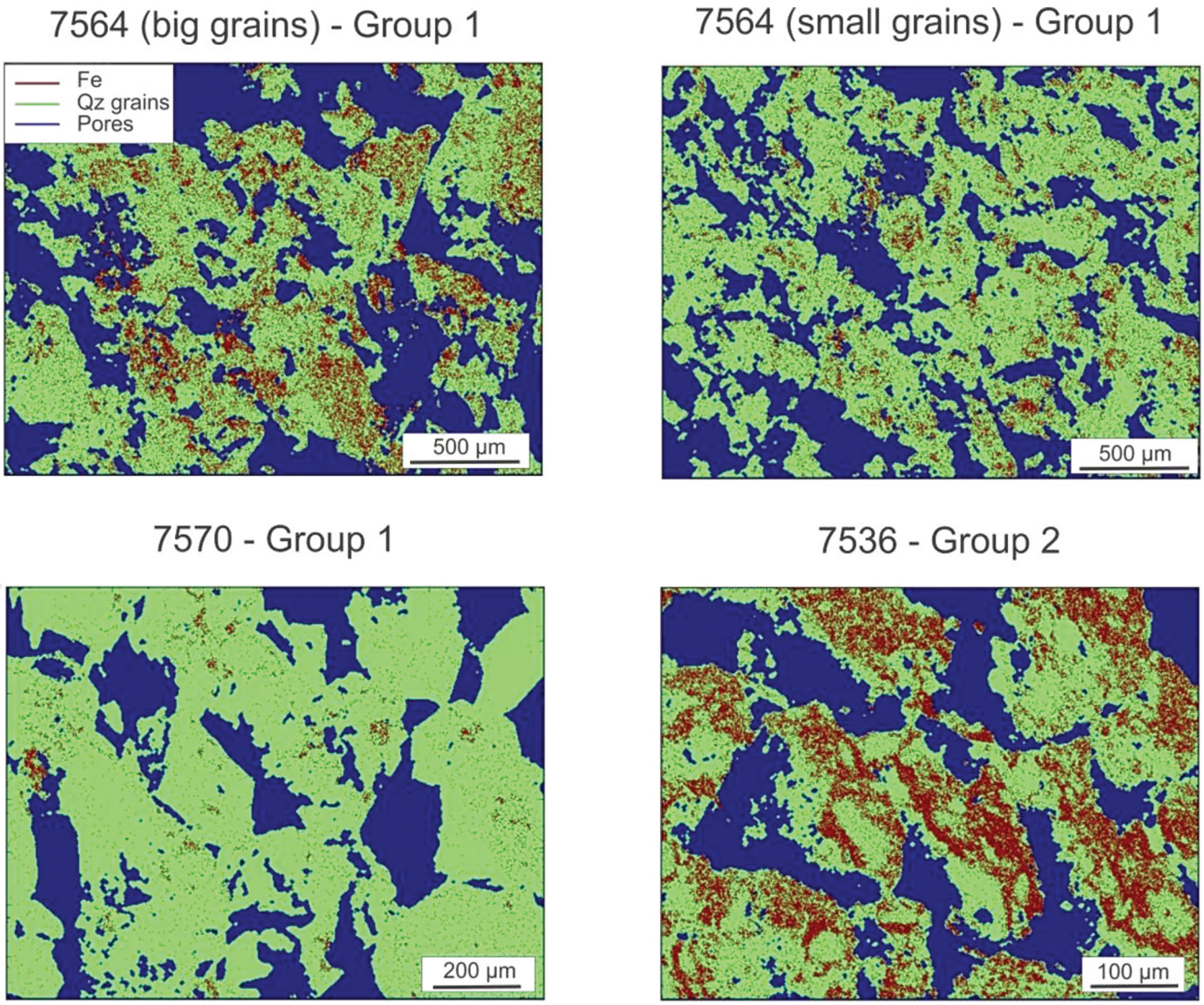

Fig. 3—SEM compositional maps showing low iron content on quartz host grains of Group 1 samples and higher iron content in Group 2 samples. Sample 7570 is also characterized by the lowest values of magnetic susceptibility.

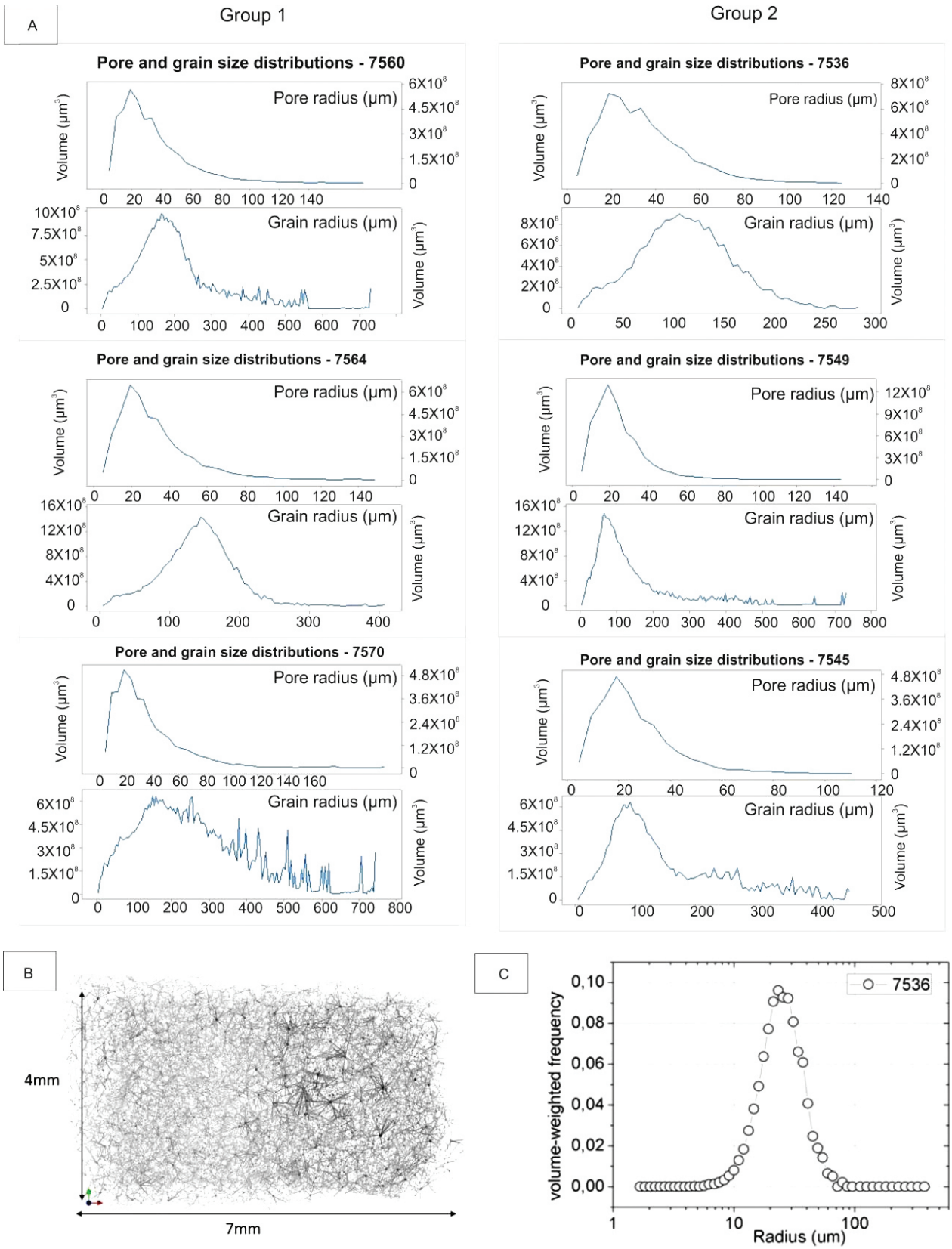

Fig. 4—μCT images showing pore and grain distributions for Group 1 and Group 2 reservoir samples (a). (b) A network visualization method used for Sample 7536 indicates lamination; and (c) a histogram of pore-volume distribution.

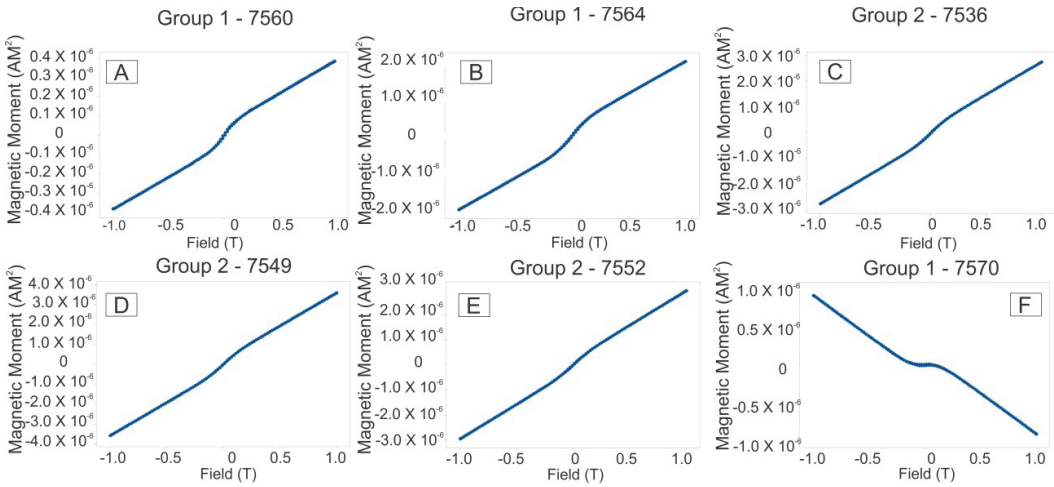

Fig. 5—Curves of magnetic field (T) against magnetic moment (A.m)—hysteresis loop—for reservoir samples showing a dominant paramagnetic behavior for Groups 1 and 2, except for Sample 7570, which is dominantly diamagnetic at higher fields. All samples show some content of low-coercive ferromagnetic particles, probably magnetite, as indicated by the magnetic hysteresis.

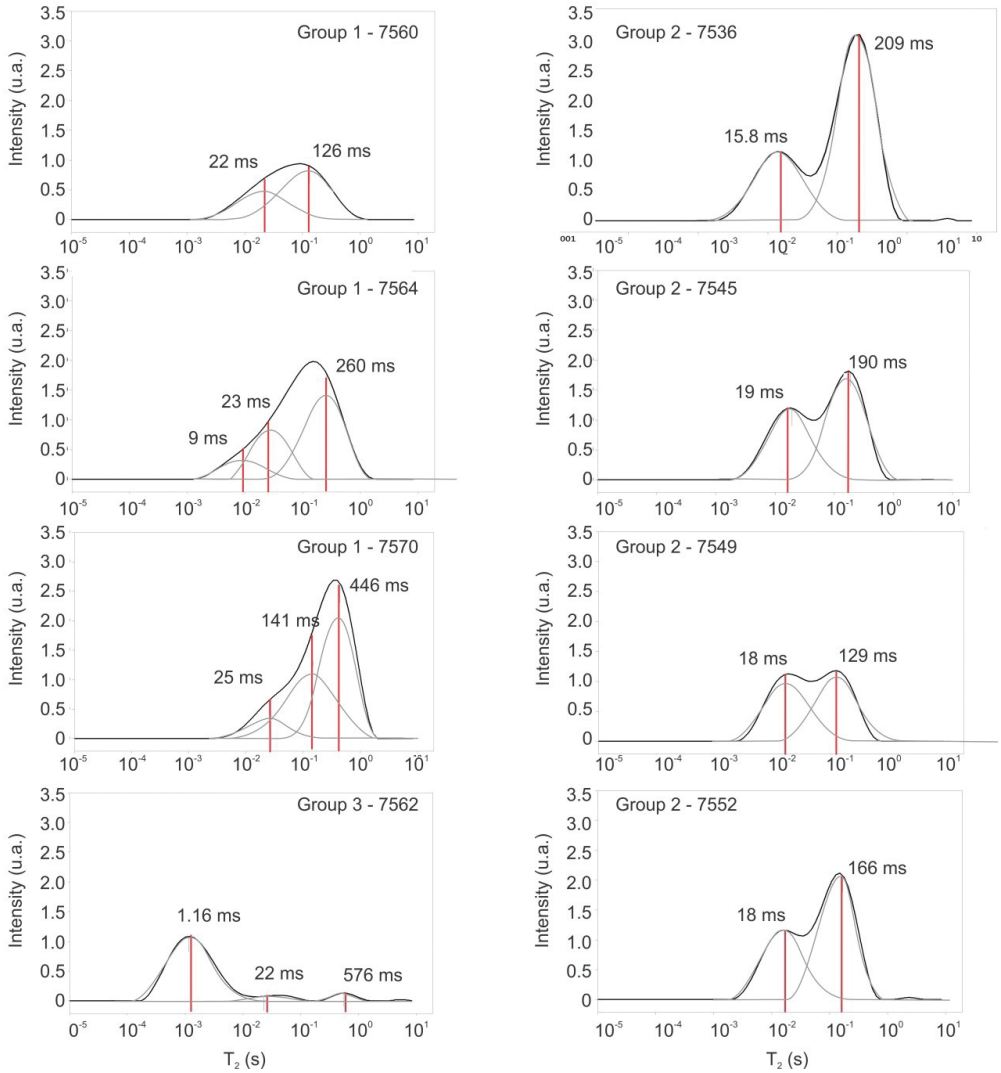

Fig. 6— T_2 distributions for Groups 1, 2 and 3. Group 1 samples (left column, except Sample 7562) shows a wide NMR T_2 distribution. Group 2 samples (right column) show bimodal distributions. The nonreservoir sample (Group 3, left column and last line) shows an intense peak in shorter times.

It can be observed that Group 1 longest T_2 times are higher than those of Group 2. To verify if this effect is related to internal magnetic field gradients around the pore surfaces, we can compare measurements performed for samples of both Groups using low- (2 MHz) and high- (85 MHz) field NMR (Fig. 7). All reservoir samples show an increase of the shortest amplitudes in the 85-MHz field. Group 1 samples present fewer displacements between the two curves than Group 2, for which longer T_2 peaks present displacements to shorter times by a factor of 10 in the 85-MHz high field. This shift is due to internal gradients in a high magnetic field, caused mainly by the differences in magnetic susceptibility between the pore surface and fluid. In this turn, the internal gradient is negligible in a low external magnetic field, such as 2 MHz (Song et al., 2002). The 85-MHZ field internal gradients are estimated on the order of 10^2 to 10^3 (Gauss/cm) for large pores (longest T_2) and 10^3 (Gauss/cm) for smallest pores, as it expected (Song et al., 2002). These differences

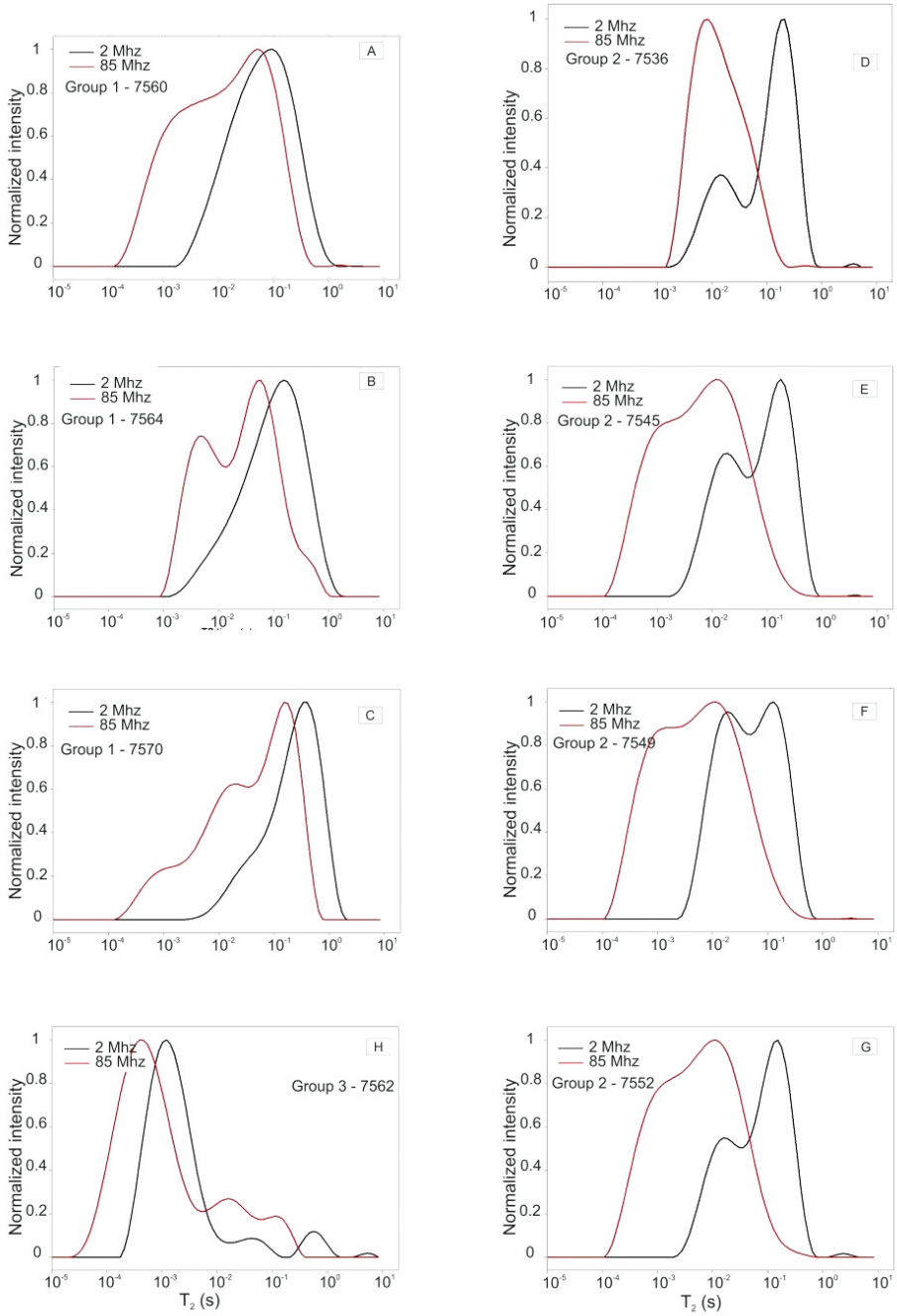

Fig. 7—2-MHz and 85-MHz T_2 distributions for Groups 1, 2 and 3 (a to h).

are due the differences in protons traveling around shorter average distances in small pores when compared to those in larger pores, where there are particles near and far from pores surface. Besides this, NMR experiments increasing the time between π RF pulses from 200 to 500 μs in low magnetic field (2 MHz) were also performed and do not show significant displacements of T_2 curves, which evidences the minimization of the internal gradient effect using 200 μs as the echo time. Group 3 sample also shows a small displacement between the 2- and 85-MHz curves due to the very low water content that fills its pores (Fig. 7d).

D-T_2 maps for representative reservoir samples are shown in Fig. 8. The nonreservoir sample did not show meaningful results due to its very low porosity. Group 1 and Group 2 samples show very similar behaviors for the diffusion on their macropores, which are defined by time of diffusion for 40 ms. Using the PFG-STE method, during the diffusion time, the magnetization is on longitudinal axis and the relaxation is by T_1, which minimizes the loss of magnetization during this time (Tanner, 1970). So, this result presents only pores with relaxation times greater than the diffusion time. The longest T_2 time is closer to the bulk water translational diffusion coefficient. This is compatible with the dominance of larger pores. The shortest T_2 is correlated with the lower translational diffusion coefficient and indicates restricted diffusion from the smaller pores into the macropore range.

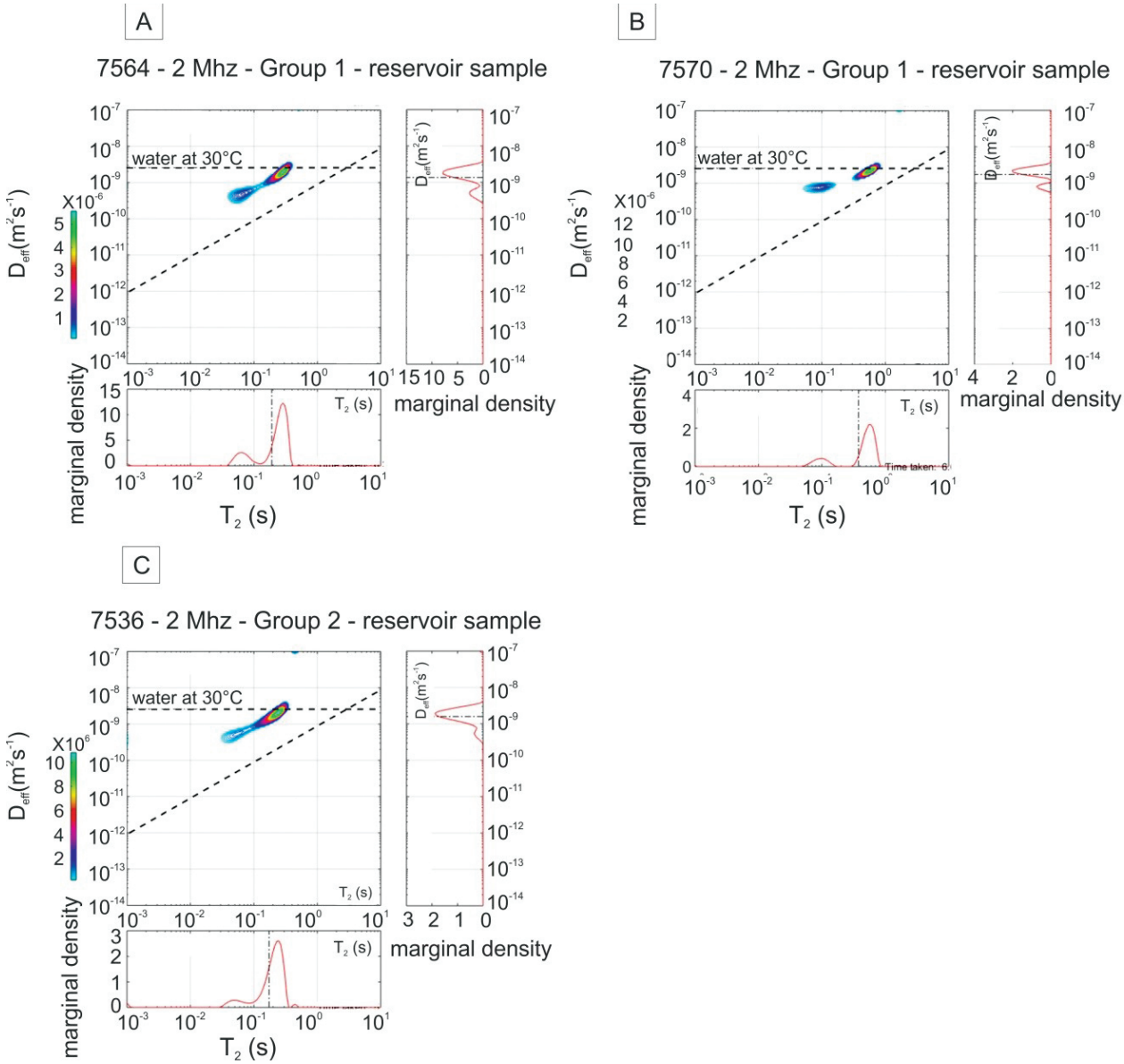

Fig. 8—*D*-T_2 maps with 40-ms diffusion time for representative samples of all Groups.

DISCUSSION

Intergranular and Secondary Porosity

Samples present heterogeneities at the hand-sample and thin-section scales that could be responsible for part of the observed NMR responses. The three groups of samples from the Água Grande formation studied here present particular characteristics at different scales. Group 1 samples present fining-upwards texture, relatively lower content of chlorite coating, lower magnetic susceptibility, smaller porosity values and wider T_2 distributions. Group 2 samples show well-defined parallel laminations, higher content of chlorite coating, relatively higher magnetic susceptibility, larger porosity values and bimodal T_2 distributions. Group 3 corresponds to the nonreservoir Sample 7562, which is highly cemented sandstone with almost no porosity. It has higher values of magnetic susceptibility and microporosity is predominant over macroporosity, according to the NMR data.

In the macropore range, the NMR T_2 values of Group 1 samples are higher than those observed for Group 2 samples. However, contrary to what would be expected, the first group shows lower porosity. NMR measurements can be affected by the presence of magnetic gradients at the pore surface. Higher internal magnetic field gradients due to the paramagnetic chlorite are known to shift T_2 values to shorter relaxation times (Kleinberg et al., 1994; LaTorraca et al., 1995; Rueslatten et al., 1998). In addition, clays generate micropores that also cause faster relaxation (LaTorraca et al., 1995). In our samples, the paramagnetic chlorite coating controls the low magnetic susceptibility, therefore, an internal gradient could be expected for samples with a higher content of grain coating in high magnetic fields. This effect is observed in Fig. 7, when we compare 2-MHz and 85-MHz T_2 distributions for low-susceptibility samples of Group 1 and high-susceptibility samples of Group 2.

The T_2 shift to lower values for Group 1 samples is much less pronounced than in Group 2. Moss and Jing (2001) showed similar shifts to shorter T_2 times in smectite-bearing samples. They associated this effect to smectite expansion due to water infiltration between clay layers. Since our samples are devoid of smectite or other expansible clay minerals, the observed shift must be caused by other factors, such as different pore sizes or diffusive coupling. It is also interesting to note that T_2 distributions obtained with different times between π RF pulses in a 2-MHz field for Group 2 samples, which show the highest magnetic susceptibilities, do not vary. This result implies that at low fields the magnetic-field inhomogeneities do not affect the T_2 distribution significantly, at least for the chlorite contents of the studied Água Grande reservoir rocks. These results are different from those obtained by Zhang et al. (2001) who interpreted the shift to be caused by an internal field gradient in the chlorite-bearing sandstones.

NMR responses for macropores can also be compared with μCT results (Fig. 4). This technique has a 5-μm spatial resolution and thus suited only to image the macropores. Results show that both Group 1 and Group 2 samples present similar pore-size distributions and the longest T_2 peaks (≥ 0.1 s) are correlated to the intergranular macropores whose modes are centered at 30 μm for both groups.

Both groups of reservoir samples showed two regions with restricted diffusion on D-T_2 maps (Fig. 8). During the evolution of diffusion, the particles continue to relax by the effect of T_1, the micropores whose T_1 times are smaller than diffusion time are not measurable (Schmidt-Rohr and Spiess, 1994). The time used for diffusion was 40 ms, therefore these result represent only the macropores. The longest T_2-restricted diffusion is due to intergranular macropores, while the shortest T_2-restricted diffusion is here interpreted as a result of the secondary porosity related to dissolution of feldspar and clay intraclasts. The peak related to dissolution of feldspar is sometimes as important as that of free water. This is evidenced with Sample 7560, whose T_2 relaxation distributions show a unimodal curve, whereas dissolution of feldspar is represented by T_2 peaks at 0.022 and 0.063 s with magnitudes close to that of intergranular macropores (Fig. 6). Sample 7560 has 10.4% porosity, of which 5% is due to feldspar dissolution. On the T_2 distributions, the secondary porosity appears mainly on Group 1 samples associated with the low-intensity 0.01 s peak.

Feldspar dissolution is also present in Group 2 samples, so we interpret that the intermediated peak will also be present in Group 2 as in Group 1, however the displacement of the longest T_2 peak to shorter times in Group 2 samples could mask it. Thin sections show that feldspar pore sizes vary from 4 μm to a maximum of 30 μm in Sample 7560 where detrital feldspar was extensively dissolved.

All samples present pore-filling kaolinite/dickite grains that range in size from <1 to 5 μm and form a secondary microporosity (see Appendix 2). Kenyon (1997) defined micropores as having relaxation times $T_2 \leq 0.01$ s, therefore we interpret the T_2 peak of ~ 0.01 to 0.025 s as due to kaolinite/dickite and chlorite coatings.

Chlorite Coatings and Pore Coupling

Compositional maps (Fig. 3) showed a higher percent iron on grain surfaces of samples with more intense peaks in this T_2 time range (~0.01 s). Thus, the microporosity due to chlorite coatings can be related to the shortest reservoir T_2 times. The nonreservoir sample, on the other hand, shows a high NMR T_2 intensity peak at much shorter times (0.001

s). This rock presents almost no porosity, so very short T_2 is interpreted as due to clay-bound water of clay pore-filling, which is in agreement with the interval proposed by Straley et al. (1995) and Kausik et al. (2011), who define T_2 of ≤ 3 ms and ~1 ms as due to clay-bound water.

Several studies have shown the effect of pore coupling on NMR relaxation (e.g., Straley et al., 1995; Kenyon, 1997; Zhang et al., 1998, 2001; Anand and Hirasaki, 2005). Chlorite flakes, which are the coating on the studied sandstones, are modeled in terms of their NMR response as microchannels perpendicular to the pore walls, forming micropores connected with the adjacent macropore (Straley et al., 1995; Kenyon, 1997) (Fig. 9).

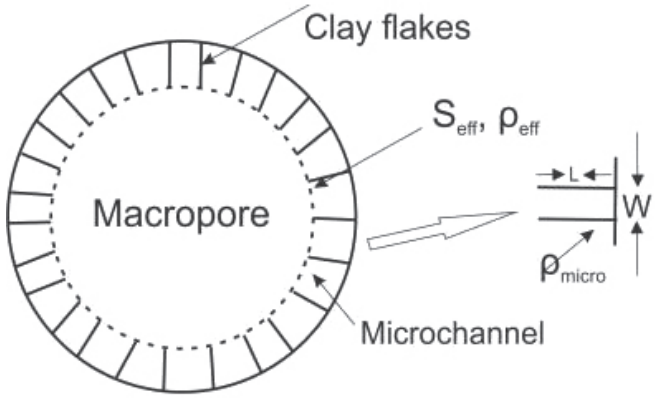

Fig. 9—Model for diffusion coupling (adapted from Kenyon, 1997).

The diffusion of protons from macropores to micropores affects the NMR response but not always in a uniform manner. Kenyon (1997) described two models for the NMR response according to the degree of coupling between clay flakes, connected channels, and central macropores. When diffusion coupling is not observed, two different relaxation times appear at the T_2 distribution, the shorter one correlates with the width of chlorite channels and the longer one correlates with the macropores.

When diffusion coupling is very efficient, the magnetization of the whole pore is uniform, both in the channels and in the center of the macropore. In this case, only one relaxation time is obtained and the system is at the fast-diffusion limit. However, the *S/V* will increase due to the roughness of the pore surface induced by the presence of the clay flakes, causing a decrease in T_2 values. According to Anand and Hirasaki (2005) the intermediate coupling is characterized by two distinct modes, which are correlated with distinct pores, but the intensities of the T_2 distribution peaks are not correlated with the true porosity values. In this case, the diffusion is fast enough to couple some micropores, but not all of them.

The NMR T_2 relaxation distributions for Água Grande reservoir samples suggest an intermediate diffusion coupling. In these samples, the T_2 peak at 0.01 s is not proportional to porosity and presents a significant displacement towards the T_2 of macropores. Figure 3 shows qualitatively that the content of iron on quartz grains has a good correlation with the intensities of the NMR peak at 0.01 s. Anand and Hirasaki (2005) also recognized by in chlorite coated sandstones from North Burbank and described an intermediate coupling for water and strong coupling for hexane. Zhang et al. (2001) also studied rocks of this region. They described internal field gradients in NMR measurements from chlorite-coated sandstones by modifying the echo time, in an experiment similar to the one performed here. They obtained a T_2 ~0.008 s for micropores due to chlorite coating and T_2 ~0.06 s for the macropores for brine-saturated samples. Before that, Zhang et al (1998) calculated the surface relaxivity for T_2 at short echo spacing (0.2 ms) (the same echo time used in this paper) and obtained 84 ±13.0 μm/s.

Compared to the fast-diffusion case, in intermediate diffusion the time that one particle diffuses across the pore increases relative to the wall relaxation time in the channels of chlorite flakes:

$$\frac{T_d}{T_s} = \frac{L^2/D}{W/\rho} = \frac{\rho L^2}{DW} = \frac{\rho L^2}{DW} \quad \text{(Kenyon, 1997),} \tag{5}$$

where L is the length of the chlorite channel, W is the width of the chlorite channel, ρ is the relaxivity and D is the diffusion coefficient. Thus, in the deeper and narrower part of the channels, magnetization decays faster than at the opening of the micropore.

Kenyon (1997) also proposed a model to calculate the relaxivity for this behavior:

$$\rho_{eff} = \sqrt{\frac{\rho_{micro} D}{W}} \tag{6}$$

where ρ_{eff} is the effective relaxivity determined for the macropores, ρ_{micro} is the microscopic surface relaxivity, D is the diffusion coefficient of water in clay layers, and W is the separation of clay layers (Fig. 9).

Figures 1f, 1g and 1h show that channels of chlorite flakes in Água Grande reservoir samples present L = ~5 μm and W = ~5 to 10 μm, Group 2 samples showing much higher contents of coating then Group 1 sample.

We first estimate the relaxivity of the sample with the lowest coating contents, Sample 7570, for which a fast-diffusion model can be assumed. From Eq. 1, the surface relaxivity for macropores in this sample is 27.54 μm/s and the relaxivity of micropores due to chlorite is 100 μm/s.

The effective surface relaxivity for macropores in the other samples can be estimated using Eq. 6 using the calculated relaxivity for the micropores, $\rho_{micro} = 100$ μm/s and $D = 10^{-6}$ cm^2/s (Kleinberg, 1996). Thus, from Eq. 6 the effective surface relaxivity in the other samples is 31. 62 μm/s.

CONCLUSIONS

Samples from Água Grande Formation can be divided into three groups according to their texture, composition, petrophysics and NMR T_2 distribution properties. Group 1 samples show fining-upward texture, a low content of chlorite coating, intermediate to low magnetic susceptibility, lower porosity and a wide distribution of NMR T_2 distribution. Group 2 samples show well-defined parallel laminations, a higher content of chlorite coating, relatively high values of magnetic susceptibility, higher porosity and bimodal NMR T_2 distributions. In the T_2 distributions of the two groups of reservoir samples the largest peak (> 0.1 s) is due to intergranular macropores, the intermediate peak is due to feldspar or clay intraclast dissolution, and the shortest peak (~0.01 s) is due to the chlorite peak, defining the three log-Gaussians or peaks. The samples of Group 2 show only two peaks because the shift of longer T_2 to shorter times hides the intermediate peak, which represents the porosity due to dissolution of the feldspar/clay intraclasts. In the nonreservoir sample used for comparison, microporosity is predominant and relates to the clay-bound water.

In chlorite-coated samples, the T_2 shift to shorter times is interpreted as due to intermediate diffusion coupling between micropores and macropores. This drift to shorter T_2 could be an indicative of clay coatings on well-logging tools if the considered stratigraphic intervals present comparable pore-size distributions.

ACKNOWLEDGMENTS

The authors acknowledge CNPq for Marta Jácomo's scholarships. The authors thank PETROBRAS and ANP for providing the samples and Schlumberger for the La Place Inversion routines.

NOMENCLATURE

Abbreviations

CPMG = Carr-Purcell-Meiboom-Gill sequence
ILT = inverse LaPlace transform
μCT = X-ray microcomputed tomography (micro-CT)
PFG-STE = pulsed field gradient-stimulated echo
TOC = total organic carbon
XRD = X-ray diffraction

Symbols

D = diffusion coefficient
G = magnetic field gradient
L = length of mineral (chlorite) channel
M_i = equilibrium magnetization
S/V = surface/volume ratio
T_1 = longitudinal relaxation time
T_2 = transversal relaxation time
$T_{2diffusion}$ = relaxation rate due to molecular diffusion
TE = interecho time
W = width of mineral (chlorite) channel
ρ_1 = relaxitivity for longitudinal relaxation time
ρ_2 = relaxitivity for transversal relaxation time
ρ_{micro} = relaxitivity for micropore
ρ_{eff} = effective relaxivity for macropores
γ = gyromagnetic ratio
ϕ = porosity

REFERENCES

Ajdukiewicz, J.M., and Larese, R.E., 2012, How Clay Grain Coats Inhibit Quartz Cement and Preserve Porosity in Deeply Buried Sandstones: Observations and Experiments, *AAPG Bulletin*, **96**(11), 2091–2119. DOI: 10.1306/02211211075.

Anand V., and Hirasaki G., 2005, Diffusional Coupling Between Micro and Macroporosity for NMR Relaxation in Sandstones and Grainstones, Paper KKK, *Transactions, SPWLA 46th Annual Logging Symposium*, New Orleans, Louisiana, USA, 26–29 June.

Andreeta, M.B., 2017, Topological Study of Reservoir Rocks and Acidification Processes Using Complex Networks Methods, unpublished PhD thesis, Instituto de Física de São Carlos. Universidade de São Paulo. https://www.google.com/url?sa=t&rct=j&q=&esrc=s&source=web&cd=1&ved=0ahUKEwjq0b_F_NzZAhUDXlMKHXp0CscQFggwMAA&url=http%3A%2F%2Fwww.teses.uspbr%2Fteses%2Fdisponiveis%2F76%2F76132%2Ftde-30012018-154357%2Fpublico%2FMarianeBarsiAndreeta_DO_corrigida.pdf&usg=AOvVaw1fkjXZ _4HIitEN58kbkTC3. Accessed March 8, 2018.

Anjos, S.M.C., De Ros, L.F., and Silva, C.M.A. 2003, Chlorite Authigenesis and Porosity Preservation in the Upper Cretaceous Marine Sandstones of the Santos Basin, Offshore Eastern Brazil, Chapter 13 *in* Worden, R.H. and Morad, S., Editors, *Clay Mineral Cements in Sandstones*, International Association of Sedimentologists Special Publications, **34**, 291–316, Blackwell Science. ISBN: 1-40510-587-0. DOI: 10.1002/9781444304336ch13.

ANP, 2016, ANP website. http://www.anp.gov.br/wwwanp/image/publicacoes/boletins-anp/Boletim_Mensal-Producao_Petroleo_Gas_Natural/boletim_de_outubro-2016.pdf. Accessed March 22, 2018.

Beaufort D., Baronnet A., Lanson B., and Meunier A., 1997, Corrensite: A Single Phase or a Mixed-Layer Phyllosilicate

in the Saponite-to-Chlorite Conversion Series? A Case Study of Sancerre-Couy Deep Drill Hole (France). *American Mineralogist*, **42**, 109–124. http://www.minsocam.org/msa/AmMin/TOC/Articles_Free/1997/Beaufort_p109-124_97.pdf. Accessed March 8, 2018.

Berger A., Gier S., and Krois, P., 2009, Porosity-Preserving Chlorite Cements in Shallow-Marine Volcaniclastic Sandstones: Evidence from Cretaceous Sandstones of the Sawan Gas Field, Pakistan, *AAPG Bulletin*, **93**(5), 595–615. DOI: 10.1306/01300908096.

Billault V., Beaufort D., Baronnet A., and Lacharpagne J.C., 2003, A Nanopetrographic and Textural Study of Grain-Coating Chlorites in Sandstone Reservoirs, *Clay Minerals*, **38**(3), 315–328. DOI: 10.1180/0009855033830098.

Bloch S., Lander, R.H., and Bonnell, 2002, Anomalously High Porosity and Permeability in Deeply Buried Sandstone Reservoirs? Origin and Predictability, *AAPG Bulletin*, **86**(2), 301–328.

Brownstein, K.R., and Tarr, C.E., 1979, Importance of Classical Diffusion in NMR Studies of Water in Biological Cells, *Physical Review A*, **19**(6), 2446–2453. DOI: 10.1103/PhysRevA.19.2446.

Cortez, M.M.M., 1996, Geostatistical Analysis of the External Geometry of the Fluival and Eolian Reservoirs of the Água Grande Formation, central area of the Recôncavo Basin [in Portuguese], unpublished MS thesis, Universidade Estadual de Campinas, Instituto de Geosciencias Geoengenharia de Reservatorios, UNICAMP. http://repositorio.unicamp.br/handle/REPOSIP/287188. Accessed March 8, 2018.

Ehrenberg, S.N., 1993, Preservation of Anomalously High Porosity in Deeply Buried Sandstones by Grain-Coating Chlorite: Examples From the Norwegian Continental Shelf, *AAPG Bulletin*, **77**(7), 1260–1286.

Kausik, R., Minh, C.C., Zielinski, L., Vissapragada, B., Akkurt, R., Song, Y., Liu, C., Jones, S., and Blair, E., 2011, Characterization of Gas Dynamics in Kerogen Nanopores by NMR, Paper SPE-147198 presented at the SPE Annual Technical Conference and Exhibition, Denver, Colorado, USA, 30 October–2 November. DOI: 10.2118/147198-MS.

Keating K., and Knight R., 2007, A Laboratory Study to Determine the Effect of Iron Oxides on Proton NMR Measurements, *Geophysics*, **72**(1), E27–E32. DOI: 10.1190/1.2399445.

Kenyon, W., 1997, Petrophysical Principles of Applications of NMR Logging, *The Log Analyst,* 38(2), 21– 43.

Kleinberg, R.L., 1996, Utility of NMR T_2 Distributions, Connection With Capillary Pressure, Clay Effect, and Determination of the Surface Relaxivity Parameter ρ_2, *Magnetic Resonance Imaging*, **14**(78), 761–767. DOI: 10.1016/S0730-725X(96)00161-0.

Kleinberg, R.L., Kenyon, W.E., and Mitral, P.P., 1994, Mechanism of NMR Relaxation of Fluids in Rock, *Journal of Magnetic Resonance Series A*, **108**(2), 206–214. DOI: 10.1006/jmra.1994.1112.

LaTorraca, G.A., Dunn, K.J., and Bergman, D.J., 1995, Magnetic Susceptibility Contrast Effects on NMR T_2 Logging, Paper JJ, *Transactions, SPWLA 36th Annual Logging Symposium*, Paris, France, 26–29 June.

Leite, C.M.M., Almeida, J.R., and De Ros L.F., 2014, Preservation of microquartz porosity in eolian reservoirs of the Água Grande formation, Recôncavo Basin, Bahia [in Portuguese], Paper 016233 presented at the 47th Brazilian Geological Congress, Salvador, Bahia, Brazil, 21–26 September.

Luo, J., Morad, S., Salem, A., Ketzer, J.M., Lei, X.L., Guo, D.Y., and Hlal, O., 2009, Impact of Diagenesis on Reservoir-Quality Evolution in Fluvial and Lacustrine-Deltaic Sandstones: Evidence From Jurassic and Triassic Sandstones From the Ordos Basin, China, *Journal of Petroleum Geology*, **32**(1), 79–102. DOI: 10.1111/j.1747-5457.2009.00436.x.

Magnavita, L.P., Szatmari, P., Cupertino, J.A., Destro, N., and Roberts, D., 2012, The Recôncavo Basin, *in* Roberts, D.G., and Bally, A.W., Editors, *Regional Geology and Tectonics: Principles of Geologic Analysis*, Elsevier. ISBN: 9780444530424.

McKinley, J.M., Worden, R.H., and Ruffell, A.H., 2003, Smectite in Sandstones: A Review of the Controls on Occurrence and Behavior During Diagenesis, Chapter 5, *in* Worden, R.H., and Morad, S., Editors, *Clay Mineral Cements in Sandstones*, International Association of Sedimentologists Special Publication **34**, Blackwell Publishing, 109–128. ISBN: 1-40510-587-0. DOI: 10.1002/9781444304336.ch5.

Milani, E., and Davison, I., 1988, Basement Control and Transfer Tectonics in the Reconcavo-Tucano-Jatoba Rift, Northeast Brazil, *Tectonophysics*, **154**(1–2), 41–50, 53–70. DOI: 10.1016/0040-1951(88)90227-2.

Mitchell, J., Chandrasekera, T.C., Holland, D.J., Gladden, L.F., and Fordham, E.J., 2013, Magnetic Resonance Imaging in Laboratory Petrophysical Core Analysis*, Physics Reports,* **526**(3), 165–225. DOI: 10.1016/j.physrep.2013.01.003.

Morad, S., Ketzer, J.M., and De Ros, L.F., 2000, Spatial and Temporal Distribution of Diagenetic Alterations in Siliciclastic Rocks: Implications for Mass Transfer in Sedimentary Basins, *Sedimentology*, **47(**Supplement 1), 95–120. DOI: 10.1046/j.1365-3091.2000.00007.x.

Moraes, M.A.S., and De Ros, L.F., 1990, Depositional, Infiltrated and Authigenic Clays in Fluvial Sandstones of the Jurassic Sergi Formation, Recôncavo Basin, Northeastern Brazil, *in* Houseknecht, D.W., and Pittman, E.D., Editors, *Origin, Diagenesis, and Petrophysics of Clay Minerals in Sandstones*, SEPM Special Publications, **47**, 197–208. DOI: 10.2110/pec.92.47.0197.

Moss, A.K., and Jing, X.D., 2001, An Investigation Into Effect of Clay Type Volume and Distribution on NMR Measurements in Sandstones, Paper SCA2001-29 presented at the SCA International Symposium, Edinburgh, Scotland, UK, 17–19 September.

Pittman, E.D., Larese, R.E., and Heald, M.T., 1992, Clay Coats: Occurrence and Relevance to Preservation of Porosity in Sandstones, *in* Houseknecht, D.W., and Pittman, E.D., Editors, *Origin, Diagenesis, and Petrophysics of Clay Minerals in Sandstones*, SEPM Special Publications, **47**, 241–255. DOI: 10.2110/pec.92.47.0241.

Rueslatten, H., Eidesmo, T., Lehne, K.A., and Relling O.M., 1998, The Use of NMR Spectrometry to Validate NMR Logs

From Deeply Buried Reservoir Sandstones, *Journal of Petroleum Science and Engineering*, **19**(1–2), 33–43. DOI: 10.1016/S0920-4105(97)00033-8.

Schmidt-Rohr, K., and Spiess, W., 1994, *Multidimensional Solid-State NMR and Polymers*, Academic Press. ISBN: 97800 80925622.

Song, Y-Q., Venkataramanan, L., Hurlimann, M.D., Flaum, M., Frulla, P., and Straley, C., 2002, T_1-T_2 Correlation Spectra Obtained Using a Fast Two-Dimensional LaPlace Inversion, *Journal of Magnetic Resonance*, **154**(2), 261–268. DOI: 10.1006/jmre.2001.2474.

Srodon, J., 1980, Precise Identification of Illite/Smectite Interstratifications ny X-Ray Powder Diffraction, *Clays and Clay Minerals*, **28**(6), 401–411. http://www.clays.org/journal/archive/volume%2028/28-6-401.pdf. Accessed March 8, 2018.

Straley, C., Morriss, C.E., Kenyon, W.E., and Howard, J.J., 1995, NMR in Partially Saturated Rocks: Laboratory Insights on Free Fluid Index and Comparison With Borehole Logs, *The Log Analyst*, **36**(1), 40–56.

Tanner, J.E., 1970, Use of the Stimulated Echo in NMR Diffusion Studies, *Journal of Chemical Physics*, **52**, 2523–2526. DOI: 10.1063/1.1673336.

Washburn, K.E., Eccles, C., and Callaghan, P.T., 2008, The Dependence on Magnetic Field Strength of Correlated Internal Gradient Relaxation Time Distributions in Heterogeneous Materials, *Journal of Magnetic Resonance*, **194**(1), 33–40. DOI: 10.1016/j.jme.2008.05.025.

Wiederkehr, F., 2010, Tectono-Stratigraphic Analysis of the Itaiparica and Água Grande Formations (Recôncavo Basin Bahia) [in Portuguese], unpublished MS thesis, Federal University of Rio Grande do Sul, Institute of Geosciences, Graduate Program in Geosciences. http://hdl.handle.net/10183/28182. Accessed March 8, 2018.

Wilson, M.J., Wilson, L., and Patey, I., 2014, The Influence of Individual Clay Minerals on Formation Damage of Reservoir Sandstones: A Critical Review With Some New Insights, *Clay Minerals*, **49**, 147–164. DOI: 10.1180/claymin.2014.049.2.02.

Worden, R.H., and Morad, S., 2003, Clay Minerals in Sandstones: Controls on Formation Distribution and Evolution, Chapter 1, *in* Worden, R.H., and Morad, S., Editors, *Clay Mineral Cements in Sandstones*, International Association of Sedimentologists Special Publication **34**, Blackwell Publishing, 3–41. ISBN: 1-40510-587-0. DOI: 10.1002/9781444304336.ch1.

Zhang, G.Q., Hirasaki, G.J., and House, V., 2001, Effect of internal Field Gradients on NMR Measurements. *Petrophysics*, **42**(1), 37–47.

Zhang, Q., Lo, S.-W., Huang, C.C., Hirasaki, G.J., Kobayashi, R., and House, W.V., 1998, Some Exceptions to Default NMR Rock and Fluid Properties, Paper FF, Transactions, SPWLA 39th Annual Logging Symposium, Keystone, Colorado, USA, 26–29 May.

APPENDIX 1: METHODS

Transmitted-Light Optics

Blue epoxy-impregnated thin sections were examined with transmitted-light optical microscope to identify the minerals, the textural framework and the presence and nature of cements. The microporosity was characterized with scanning electron microscopy due to microscope resolution.

Scanning Electron Microscopy (SEM)

We used the INSPECT F50 FEI scanning electron microscope from the Instituto de Física de São Carlos, Universidade de São Paulo, to identify and characterize the clay coatings on detrital host grains and measure the pore size. Energy dispersive spectroscopy (EDS) was used for semiquantitative chemical mapping of O, Al, Fe, Mg and Si.

Porosity (ϕ) and Permeability (k) Measurements

Porosity and permeability were measured on each sample. Porosity was determined using three methods: thin-section point counting, helium-expansion at 2,500 psi and density after saturation (Table 1). Values obtained with the different methods present a good correlation. The permeability was determined using a Hassler cell (Table 1). A Core lab helium permeameter (model n. 3020-124 and serie A7520) from Petrobras/SA was used for measurements.

X-Ray Microcomputed Tomography (Micro-CT)

X-ray micro-CT (μCT) allowed the three-dimensional visualization of the pore structure of samples and estimation of pore-size distribution. In addition, the porosity also was obtained by this method. Measurements were performed with a SkyScan 1272 scanner by Bruker (USA) from Instituto de Física de São Carlos, Universidade de São Paulo, and were analyzed using the Bruker μCT software (CTAn). Samples correspond to fragments of about 0.005 cm^3 in volume collected directly from the original samples.

X-Ray Diffraction (XRD)

Clays are very common components of sedimentary rocks, but identifying them is not always a trivial task due to the variable range of physicochemical properties of clay minerals, including their composition, morphology, grain size, swelling and cation exchange (Wilson et al, 2014). Thus, X-ray diffraction is a useful technique to distinguish clays, mainly smectite and its mixed-layer, based on their expansion with ethylene glycol. Here, a Bruker D8 Advance Da Vinci Diffractometer from the Instituto de Geociências da Universidade de São Paulo (IGc/USP) was used to identify the types of clays present in the samples.

Magnetic Susceptibility and Hysteresis

Magnetic susceptibility differences within the rock samples caused by the presence of paramagnetic minerals or impurities can induce field inhomogeneity in the pore space, causing an increase in $1/T_2$ relaxation rates (Kenyon, 1997; Keating and Knight, 2007; Washburn et al., 2008). Thus, these measurements are important to understand eventual contrasts on the T_2 NMR response in the porous media. We used the Susceptmeter KLY-4S-Kappabridge by AGICO operating at 976 Hz at the Laboratório de Paleomagnetismo da Universidade de São Paulo (USPmag). Hysteresis measurements were used to investigate whether (a) the magnetic susceptibility was carried by ferromagnetic or paramagnetic minerals, and (b) the relative contribution of each magnetic phase. Measurements were performed in a Princeton Measurements Corp. vibrating sample magnetometer with a peak field of 1 T also from USPmag.

APPENDIX 2

Table A2.1—Compositional Analysis of Samples (%)

Group		1			2				3
Minerals		7560	7564	7570	7536	7545	7549	7552	7562
Primary Minerals	quartz	87.85	87.45	89.39	82.37	83.86	90.03	85.78	56.00
	plagioclase	1.96	2.96	1.10	4.63	4.57	0.43	3.26	8.00
	perthite	0.39	0.74	0.36	0.42	0.41	0.43	0.82	0.33
	microcline	0.00	0.00	0.00	0.00	0.00	0.00	0.40	0.00
Diagenetic Minerals	caulinite (dickite)	3.00	2.96	3.33	4.0	3.33	2.33	4.00	6.67
	quartz	1.56	2.67	3.30	0.42	0.41	0.87	0.40	0.00
	chalcedony	0.79	0.00	0.00	0.42	0.00	0.87	0.40	0.00
	illite/ smectite	0.00	0.00	0.00	0.00	0.00	0.00	0.00	5.00
	Illite	0.00	0.00	0.00	0.00	0.00	0.00	0.00	3.34
	anatase	0.00	0.37	0.36	1.26	0.41	0.43	0.40	4.67
	dolomite	0.00	0.00	0.00	0.00	2.90	1.74	0.82	0.00
	albite	1.96	0.00	0.00	0.00	0.83	0.43	0.82	0.00
	pyrite	0.00	0.74	0.36	0.42	0.00	0.00	0.00	2.66
Accessory Minerals	cianite	0.00	0.00	0.00	0.42	0.00	0.00	0.00	0.00
	biotite	0.00	0.00	0.36	1.26	0.83	0.00	0.40	1.67
	muscovite	0.00	0.00	0.00	0.84	0.41	0.43	0.00	1.33
	epidote	0.00	0.00	0.00	0.42	0.00	0.00	0.00	0.33
	zircon	0.39	0.37	0.00	0.42	0.00	0.43	0.82	1.00
	tourmaline	0.00	0.37	0.00	0.00	0.41	0.43	0.40	0.67
Silcrete		0.39	0.74	0.36	1.66	0.83	0.43	0.40	0.00
Pelitic Intraclasts		1.18	1.11	0.74	0.00	0.00	0.00	0.00	0.00
Mud Matrix		0.00	0.00	0.00	0.00	0.00	0.00	0.00	8.00

ABOUT THE AUTHORS

Marta Jácomo graduated in Geology at the Universidade de Brasília with a BS (2008) and MSc (2010). She is currently, a doctoral student at the Instituto de Astronomia, Geofísica e Ciências Atmosféricas/ Universidade de São Paulo. Her main researches comprise petrophysical properties applied to reservoir. She works with acquisition, processing, integration and interpretation of NMR, petrophysics and geological data.

Ricardo Trindade graduated in Geology at the Universidade Federal do Rio Grande do Norte in 1995 and received a PhD in Geophysics from the Universidade de São Paulo (1999). He was visiting professor at Université de Toulouse and Institute de Physique du Globe de Paris, both in France. He has been a full professor in the Universidade de São Paulo since 2012. His main interests are mineral and rock magnetism, and paleomagnetism applied to geological and environmental problems.

Éverton Lucas de Oliveira is a PhD student at the Instituto de Física de São Carlos, Universidade de São Paulo. He has a BSc and a MSc in Computational Physics from the same Institute. His principal area of study is nuclear magnetic resonance, with applications mainly in porous media and diffusion process.

Carlson Leite is graduated the from Universidade de Brasília in 1978, received a master's degree from the Royal School of Mines/Imperial College/University of London in 1985, and a PhD from the Universidade Federal da Bahia in tectonics and metamorphic petrology in 2002. He worked at the Baiana Mineral Research Company in between 1978–1997 and has worked at Petrobras since 2002. He has also worked as a lecturer at the Universidade Federal da Bahia since 2008, teaching structural and geotectonic geology in geology and mining engineering graduating courses. His areas of activity and research include structural geology, sedimentary petrology and structural diagenesis.

Elton Tadeu Montrazi has a BSc (2009), a MSc (2012) and a PhD (2016) from the Instituto de Física de São Carlos (IFSC), Universidade de São Paulo (USP). Currently, he is a post-doctoral fellow at the same Institute where he is using NMR to study porous media.

Mariane Barsi Andreeta graduated in Physics from the Universidade de São Paulo (2008), has a MSc degree from Universidade de São Paulo. She is currently is a doctoral student at the Instituto de Física de São Carlos. Research interests comprise data processing of digital reservoir rocks for analysis of petrophysical properties, with emphasis in topological characterization of the media through network science.

Tito Bonagamba received his BSc, MSc and PhD in Physics from the Instituto de Física de São Carlos - Universidade de São Paulo, Brazil, and pursued post-doctoral research at the University of Massachusetts (Amherst) and Iowa State University (Ames), USA. He was a researcher at Ames National Laboratory, USA, and visiting professor at Université Paris-Sud (Orsay), France, Martin-Luther University Halle-Wittenberg (Halle), Germany and Università degli Studi di Sassari, Italy. He has experience in condensed matter physics, working mainly on nuclear magnetic resonance (NMR) and its applications, including porous media. He also works in the field of NMR instrumentation.